Journal of Hydrology: Regional Studies 13 (2017) 26–42

Contents lists available at ScienceDirect

Journal of Hydrology: Regional Studies

journal homepage: www.elsevier.com/locate/ejrh

Downscaling climate projections for the Peruvian coastal Chancay-Huaral Basin to support river discharge modeling with WEAP

Taru Olsson[a,*], Matti Kämäräinen[a], Darwin Santos[b], Teija Seitola[a], Heikki Tuomenvirta[a], Riina Haavisto[a], Waldo Lavado-Casimiro[b]

[a] Finnish Meteorological Institute (FMI), PB 503, 00101, Helsinki, Finland
[b] Servicio Nacional de Meteorologia e Hidrologia del Perú (SENAMHI), Jr. Cahuide 785 Jesús María, Lima11, Peru

ARTICLE INFO

Keywords:
Bias correction general circulation model
Climate change
Hydrological modeling
Quantile mapping
Peru

ABSTRACT

Study region: The Chancay-Huaral (CH) coastal river basin in the Lima Region, Peru, between the Pacific Ocean and the Andean Cordillera.
Study focus: Climate change impacts on annual and monthly discharges in the CH Basin are assessed for the future period 2051–2080. Hydrological modeling is sensitive to biases in input variables. Therefore, bias-corrected time series of temperature and precipitation from 31 General Circulation Models (GCMs) with the emission scenarios RCP4.5 and RCP8.5 (Representative Concentration Pathways) were used as inputs for the Water Evaluation and Planning System model (WEAP). Bias correction and downscaling of the GCMs were implemented using a quantile mapping method.
New hydrological insights for the region: On average, GCMs indicate increased annual mean temperatures by 3.1 °C (RCP4.5) and by 4.3 °C (RCP8.5) and precipitation sum by 20% (RCP4.5) and by 28% (RCP8.5). With increasing total precipitation, river discharges are also found to increase, but the variability among the GCMs is considerable. The largest increases in monthly discharge are projected to occur in the wet season (November − April) − with up to 31% increase of December multi-model mean. Despite the larger annual discharge for the mean multi-model result, discharges in the dry season may decrease according to some GCMs, showing the need for an adapted future water management.

1. Introduction

The North–South Andean Cordillera divides Peru (1.3×10^6 km^2) into three watersheds (hydrographic regions, Fig. 1): one toward the Pacific Ocean (Pacific drainage, Pd), another toward the Amazon Basin, and the third is the Lake Titicaca Basin on the Altiplano to the south. According to the Peruvian National Water Agency, Pd represents 22% of the Peruvian territory (Ruiz et al., 2008). The annual water balance (precipitation minus evapotranspiration) computed by UNESCO (UNESCO, 2006) for 1969–1999

Abbreviations: BC, bias correction; CH, Chancay-Huaral; CMIP3, CMIP5, the coupled model intercomparison project phase 3/5; EHSD, Santo Domingo Hydrological Station (Estación Hidrológica Santo Domingo); ENSO, El Niño southern oscillation; EP, Eastern Pacific; FAO, United Nations Food and Agriculture Organization; GCM, general circulation model; GDP, gross domestic product; GIS, geographic information system; IPCC, Intergovernmental Panel on Climate Change; IPCC AR4, AR5, IPCC Fourth/Fifth Assessment Report; MMC, Million cubic meters; MTM, multitaper spectral analysis method; Pd, Pacific drainage; RCP, representative concentration pathways; RLS, regulated lagoon system; RMSE, root mean square error; SENAMHI, Servicio Nacional de Meteorologia e Hidrologia del Perú; SPI-6, 6-monthly standardized precipitation index; STL, loess based seasonal trend decomposition; UNESCO, United Nations Educational, Scientific and Cultural Organization; YPS, yearly sum of precipitation; YWD, yearly number of wet days; WEAP, water evaluation and planning system model

* Corresponding author.
E-mail address: taru.olsson@fmi.fi (T. Olsson).

http://dx.doi.org/10.1016/j.ejrh.2017.05.011
Received 22 September 2016; Received in revised form 11 May 2017; Accepted 26 May 2017
Available online 12 August 2017

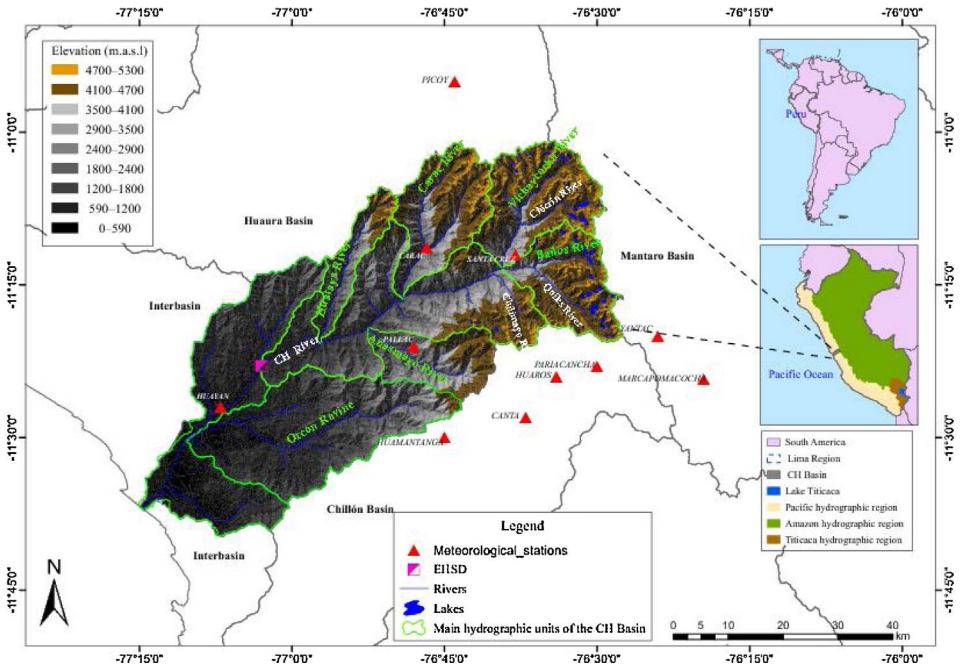

Fig. 1. Map of the location of the Chancay-Huaral Basin and adjacent basins (Huaura, Chillón, Mantaro) as well as the meteorological and hydrological stations that collected the data interpolated as input into the WEAP model. The main parameters of these observational stations are listed in Table 1. EHSD = hydrological station.

shows that the average annual available surficial water in Pd is only 16 mm. The Pd features small basins with bare and steep slopes that favor erosion and flooding during occasional rainy episodes. Rainfall is more abundant along the northern coast of Peru and declines toward the south where conditions are extremely arid (Garreaud et al., 2009).

The flow of the Chancay-Huaral (CH) River, which is recorded at the Santo Domingo Hydrological Station (*Estación Hidrológica Santo Domingo*, EHSD), plays a very important role in the economic development of the basin. The agricultural sector in the CH Basin accounts for 17% of the total gross domestic product (GDP) of the entire province of Lima (PMGRH-I, 2012). Precipitation in the upper part of the basin contributes to feeding a set of reservoirs that are discharged mainly during the dry season for hydropower purposes, agricultural use, and residential water use. In the lower part of the basin, runoff generated by seasonal rainfall supplies aquifers that are mainly used for agricultural irrigation and domestic water usage. In this regard, an uneven spatio-temporal distribution of rainfall would greatly affect water resources in this basin. For example, between 1940 and 1973, communities of the upper valley of Chancay were severely affected by five periods of drought (Lausent-Herrera, 1994).

There are increasing and competing demands on the use of water resources in Peru. The multifaceted issue of sustainable water usage and the water–food–energy security nexus has been widely acknowledged and discussed (WBCSD, 2014; WWAP, 2015). First, the population of Peru is projected to grow by 40% from 2007 to 2050, which would correspond to a population of about 40 million (PRB, 2010). Currently, 73% of the population lives in urban environments, and this proportion, as well as their living standards, is projected to increase. Therefore, domestic water usage is likely to increase rapidly. Secondly, much of the current agricultural production relies on irrigation, and consumes about 85% of the surface water in Peru (FAO, 2013). The share of agricultural water reaches 93% in the Chancay-Huaral Basin. However, the agricultural use of water depends not only on socio-economic factors and policies (e.g., land use and agricultural policy) but also on climatological and agrological conditions (e.g., land quality, crop water requirement, and evapotranspiration). Thirdly, planning for water resources management also affects industrial development, hydropower production and population health via sanitation.

Climatic variability and change pose major scientific challenges for projections of future water resources. Even with the best available Earth system models, the uncertainty surrounding future water resources may remain large. Major investments and far-reaching policy decisions regarding the development of water management may be needed to secure the future water supply and sustainable adaptation to climate change. Therefore, it is important to explore methods to project future scenarios of river discharge (discharge scenarios, hereafter) to support planning and decision-making. The studies presented in this article are part of the Peru-AquaFutura project conducted to support decision making for water resource management, including hydrological modeling and modeling of payments for watershed services (Haavisto et al., submitted).

Although it is preferable to use the most up-to-date climate models for climate change impact studies such as hydrological modeling, the raw output from low-resolution General Circulation Models (GCMs) should not be used directly to force impact models. Instead, common practice is to increase the spatial variability of GCM output data by means of statistical or dynamical downscaling. Statistical downscaling is a way to resolve the scale mismatch between local information and large-scale GCM information by applying statistical links between large-scale fields and local observations. In the dynamical downscaling approach, a regional climate

model (RCM) is run under the boundary conditions derived from a GCM. In contrast to dynamical downscaling, which is costly and still constrained by the resolution of the RCM, statistical downscaling is applicable with variety of scales starting from the station scale (Hanssen-Bauer et al., 2005). In addition, the majority of the GCMs simulate warmer and rainier climates compared with observations in the Chancay-Huaral Basin, and cannot be directly applied in impact studies because the use of uncorrected data can produce unrealistic seasonal discharges and changes. Therefore, prior to impact assessments, bias correction (BC) must be performed to adjust GCM temperature and precipitation output to better reflect the observed climate.

Distribution-based bias correction methods are more applicable for this purpose than are delta change methods (e.g., Andréasson et al., 2004; Steele-Dunne et al., 2008; Veijalainen et al., 2010), because the bias correction approach produces alternative, synthetic time series for present and future climates, whereas the delta change approach is strongly based on historical observations and does not capture changes in the temporal characteristics of climate relative to the historical period (Räisänen and Räty, 2013; Räty et al., 2014). In impact assessments, future climate variability is essential information.

We adjusted systematic biases of a 31-member subset ensemble of the CMIP5 (Coupled Model Intercomparison Project Phase 5) GCMs with a quantile mapping method (Räisänen and Räty, 2013). In this study, bias correction and statistical downscaling are performed simultaneously using local observed climate data from weather stations to adjust the large-scale GCM output. Narrowing the GCM subset by excluding the least reliable models prior to downscaling to increase the overall quality of the projections was omitted in this study mainly because the benefits of doing so are typically minor compared with those of using all available models, as shown by Räisänen and Ylhäisi (2012). However, individual model performances after bias correction were evaluated with the Standardized Precipitation Index (WMO, 2012) and other precipitation indices, which are presented in the results. Nonetheless, the multi-model mean results and inter-model variability were calculated for all 31 models. The overall performance of the bias-corrected GCM ensemble to produce observed extreme river discharges in the historical period was also estimated.

According to Intergovernmental Panel on Climate Change (IPCC) report (IPCC, 2013), El Niño Southern Oscillation (ENSO) is projected to remain the dominant mode of interannual variability with global influence in the 21 st century, and because of changes in moisture availability, ENSO-induced rainfall variability will intensify on regional scales (Christensen et al., 2013). There are indications that ENSO-induced teleconnection patterns will shift eastward over the North Pacific and North America. Nevertheless, changes in the intensity and spatial patterns of ENSO in a warmer climate remain highly uncertain (Christensen et al., 2013). The influence of ENSO on the interannual variability of rainfall and runoff in Pd has been studied, e.g., by Ropelewski and Halpert (1987); Tapley and Waylen (1990); Vuille et al. (2000); Romero et al. (2007); and Lavado-Casimiro et al. (2013). Marengo (1995) and Marengo et al. (1998) detected decreasing runoff trends during the 20th century at some gauging stations in the northern Pd area. These decreases were human-induced as they were often related to water catchments used for irrigation and domestic consumption in growing cities and agricultural zones.

In addition, increasing temperature is very likely to cause an increase in evapotranspiration, and thus alter components of the hydrological cycle, such as runoff and infiltration. These changes will have significant impacts on the water vapor content of the atmosphere, and may cause large-scale changes in rainfall patterns and the frequency of extreme events (Bates et al., 2008). For example, in the Peruvian Amazon, extreme hydrological events, such as the droughts of 1995, 1998, 2005 and 2010 and flooding in 2012, have become more frequent (Espinoza et al., 2011).

The relationship between climate and water resources can be investigated with hydrological models. Studies of the Chancay-Huaral River Basin date back to 1969, when the National Office for Natural Resource Evaluation (*Oficina Nacional de Evaluación de Recursos Naturales*) published its *Guidelines on the Policy for the Conservation of the Renewable Natural Resources in Peru* (ONERN, 1969). Other studies have focused on the assessment of surface water resources and water availability in major tributaries of the basin using semi-distributed models (MINAG, 2002, 2011). To our knowledge, no studies of the CH Basin have been published that have evaluated the impact of climate change on river discharge using the outputs of GCMs. Selection of the hydrological model depends on many factors, primarily the purpose of the study and the availability of the model (Xu, 1999). To analyze the impact of climate change on the discharge of the Chancay-Huaral River, and to improve decision-making capabilities regarding water resources management, the Water Evaluation and Planning tool (WEAP), a hydrological model that integrates water supply and demand, was employed. The WEAP model has been used in previous climate change studies in Peru, such as to evaluate the impacts of climate change on mountain hydrology (Vergara et al., 2011) and to improve the use of water for irrigation (Swiech et al., 2012).

In this study, we investigate the impacts of climate change on hydrology in the CH Basin and focus on monthly and annual mean values of temperature, precipitation and river discharge. To estimate the impact of climate change on river discharges, input from 31 bias-corrected GCMs are used to run the WEAP hydrological model. In Section 2, we introduce the study catchment, the observed and GCM data, the quantile mapping method, precipitation indices, spectral analysis, and the WEAP model. The results for bias-corrected temperature, precipitation and discharge in the past (1981–2010) and future (2051–2080) periods, as well as a short overview of the BC impacts on ENSO cycles, are then presented and discussed in Section 3, and concluding remarks are provided in Section 4.

2. Materials and methods

2.1. Study catchment

The Chancay-Huaral Basin is a narrow coastal basin with distinct microclimates because of its proximity to the Pacific Ocean and the Andean Cordillera. It has an area of 3046 km^2, and is located in the Lima Region, Peru, between latitudes of 11°00′S and 11°39′S and longitudes of 76°26′W and 77°15′W (Fig. 1). The altitudinal variation of the CH Basin ranges from sea level to up to 5300 m above sea level. The CH Basin has eight main hydrographic units, and the surface runoff of six of these units is captured and measured

Table 1
Main parameters of the selected observational stations including station name, elevation, total annual precipitation, mean annual temperature, mean annual relative humidity, mean annual wind speed, and mean annual discharge (time period 1981–2010). Stations within the study basin, Chancay-Huaral, are highlighted with gray background (data provided by SENAMHI).

Watershed	Basin	N°	Observational station	Elevation m.a.s.l.	Annual P (mm)	T (°C)	RH (%)	WS (m/s)	Q (m^3/s)
Pacific	Huaura	1	Picoy	3,075	507	9.4	77.6	1.14	-
Chancay–Huaral		2	Huayan	350	-	17.5	86.2	2.16	-
		3	Carac	2,600	382	-	-	-	-
		4	Pallac	2,570	279	-	-	-	-
		5	Santa Cruz	3,590	573	-	-	-	-
		6	Santo Domingo *	564	-	-	-	-	16
	Chillón	7	Canta	2,832	337	11.2	77.8	1.30	-
		8	Huamantanga	3,392	392	-	-	-	-
		9	Huaros	3,585	494	-	-	-	-
		10	Pariacancha	3,800	695	-	-	-	-
Amazon	Mantaro	11	Marcapomacocha	4,479	1,045	2.1	-	-	-
		12	Yantac	4,600	751	-	-	-	-

P = precipitation, T = temperature, RH = relative humidity, WS = wind speed, Q = discharge.
*EHSD = hydrological station.

at the EHSD hydrological station, with an average annual discharge of 16 m^3/s (PROFODUA, 2005). Table 1 shows the characteristics of the hydrometeorological stations in the basin.

There are uncertainties in the hydrological data of the CH Basin, which partly arise from the fact that the CH Basin has different sources for water managed by different socio-economic sectors. One of these sources is the Regulated Lagoon System (RLS), located in the upper part of the hydrographic unit Vichaycocha and Baños (showing a transfer from the Mantaro Basin, Fig. 1). The RLS has a maximum estimated storage capacity of $75 \times 10^6 m^3$, and it is administered by the Water User Board for Irrigation (*Junta de Usuarios*) of the CH Basin. The water discharge of the RLS is used for hydroelectric production and mining, and during droughts it is also used by the agricultural sector and by households. Currently, because these water resources are poorly controlled, the infrastructure of some lakes is being improved, and new gateways are being implemented to control discharge, to limit and manage the use of these water resources. Very little discharge data are available for the RLS. Therefore, it was not possible to integrate the RLS into the WEAP hydrological model. Information is somewhat limited on the sources of underground water recharged through the riverbed and irrigation systems located in the lower part of the CH Basin. According to the best information currently available (ANA, 2011), the exploitable reserves of groundwater constitute about 102×10^6 m^3/year, and the use of 3209 wells currently adds up to about 15×10^6 m^3/year.

Other sources of recovered water vital for irrigation during low-flow periods are return flow, upwelling from groundwater and natural springs, and groundwater recovered by open pit drains along the lower basin. Furthermore, rights are granted to allow the irrigation of 31% (6627 ha) of the total (21,330 ha) irrigated land (PROFODUA, 2005). It is estimated that the volume of the annual recovered waters is approximately 122 hm^3, which represents an estimated flow of 3.6 m^3/s.

2.2. Observations and GCM data

Daily meteorological observations of mean temperature and cumulative precipitation assembled from four temperature stations and 10 precipitation stations were provided by SENAMHI (*Servicio Nacional de Meteorologia e Hidrologia del Perú*, Table 1). Daily precipitation measurements from Carac, Pallac and Santa Cruz, and daily mean temperature measurements from Huayan, were used to investigate the monthly and seasonal patterns of the current climate in the CH Basin. Huayan is a coastal station at a relatively low elevation, and therefore is not representative of the whole CH Basin. Therefore, temperatures from stations located in neighboring basins, Picoy, Canta, and Marcapomacocha, are also shown in the results. All stations presented in Fig. 1 and Table 1 were used to produce reliable discharge values with the WEAP hydrological model, even though they are located outside our main area of interest, the CH Basin.

Annual mean temperatures exhibit strong local variations within the basin, with a range from 2 °C at 4479 m elevation (Marcapomacocha) to over 17 °C at the coastline (Huayan). Distinct seasonal cycles can be detected in coastal areas, whereas temperature variations are smaller inland. The accumulated annual precipitation varies from 280 mm/year on the hillside (Pallac) to 1000 mm/year in the Amazon region (Marcapomacocha). Seasonal patterns of precipitation are similar between stations. The greatest contributions of precipitation occur from December to March, which allow water storage in reservoirs (natural and regulated) and runoff in the basin.

Outputs from global climate models of the CMIP5 (Taylor et al., 2012; Flato et al., 2013) project were selected for this study because these data represent the most up-to-date and comprehensive collection of numerical climate change information. A subset of 31 climate models out of the total 39 models were used, based only on the criterion of the availability of precipitation and temperature data with daily time resolution. The GCMs are listed in Fig. 6; the abbreviations used follow the IPCC naming conventions

(http://cmip-pcmdi.llnl.gov/cmip5/docs/CMIP5_modeling_groups.pdf). Two emission scenarios, RCP4.5 and RCP8.5 (Representative Concentration Pathways, van Vuuren et al., 2011), which represent moderate and high future emissions, respectively, were employed and analyzed. The computational grid cell width of the global climate models varies between 125 and ~400 km, which makes downscaling prior to hydrological modeling necessary.

2.3. Bias correction and downscaling

A quantile mapping procedure was applied for all precipitation and temperature stations, although the results are shown only for the CH Basin (Fig. 1, Table 1). This method has been evaluated by Räisänen and Räty (2013, method M9), who reported that it showed the best skill among several bias correction methods applied to temperature data in RCMs. Simpler scaling corrections could also have been applied, as the hydrological model uses monthly time resolution, but performing corrections in daily time resolution allowed us to better investigate the characteristics of climate change using a variety of different impact indicators, such as precipitation indices.

First, the precipitation and temperature time series from the global climate models were interpolated to station locations using bilinear interpolation. Secondly, monthly correction functions were constructed for each station and for each climate model using the quantile differences between observations and modeled time series in the 1981–2010 calibration period. Specifically, the observed (F_O) and modeled (F_c) cumulative distributions were used to modify values in the modeled time series (s_i) to obtain the projection (p_i) as follows:

$$p_i = F_o^{-1}(F_c(s_i)) \cdot \quad (1)$$

Both studied time periods, 1981–2010 and 2051–2080, were projected using the same correction functions. Large proportions of observational data are occasionally missing for some stations (18% for precipitation data and 22% for temperature data, on average), which is likely to increase both the corrections and the projection uncertainties to some degree. Mixing data from surrounding months when constructing the correction functions (1) would reduce the sampling uncertainty in the extreme tails and result in more robust functions, as suggested by Räisänen and Räty (2013). As a consequence, the observed climatological monthly mean values in the calibration period are not accurately reproduced. To increase the accuracy in climatological monthly mean values we did not mix data from different months, and for the same reason, the numbers of quantiles (300 for temperature and 1000 for precipitation) were kept high, and only minor (for temperature) or no (for precipitation) smoothing was applied to the functions. Finally the climate model time series were projected using the correction functions. Prior to projection of precipitation, the limit value for dry days, pr_{LIM_MOD}, was defined for each location, month, and climate model such that the number of dry days in the calibration period matched the observed number of dry days with $pr_{LIM\_OBS} = 0.1$ mm/day, the precipitation rates below pr_{LIM_MOD} were set to zero, and projections were performed for wet days only.

2.4. Precipitation indices

Precipitation indices were first calculated separately for the three stations (Carac, Pallac and Cruz), and then averaged over all three. Because dry days are virtually missing in the uncorrected model output, only bias-corrected models were analyzed. Indices were calculated separately for all GCMs and for observations. The following indices were calculated:

2.4.1. Six-monthly standardized precipitation index

The SPI-6 index (McKee et al., 1993; WMO, 2012) uses monthly precipitation data and reflects the cumulative effect of precipitation such that a negative SPI value indicate that either (a) several dry months occur sequentially or (b) at least one month is exceptionally dry. The negative value of the index becomes large if both (a) and (b) occur together. Observed data from 1981 to 2010 (all months) were used in the calibration of this indicator. Missing months were filled with climatological monthly mean values. The six-monthly averaging window was selected because compared with shorter and longer averaging windows, it represents both agricultural and hydrological time scales rather well (WMO, 2012). From these results, April SPI values were analyzed; thus, with the six-monthly window, the wet season months from November to April, which roughly define the yearly supply of water, are taken into account.

2.4.2. Yearly number of wet days (YWD)

To increase the comparability of the modeled and observed data, the probability of wet days, $P_w = W/N \approx 0.26$ was calculated, where W is the total number of (non-missing) wet days during the reference period 1981–2010, and N is the total number of (non-missing) days in the same period. The results were then used to offset the effect of missing data in the observed YWD. The variable P_w represents the average yearly probability of the wet days calculated over the three stations, based on the assumption that the missing data are evenly distributed throughout the year.

2.4.3. Yearly sum of precipitation (YPS)

To maintain comparability between observations (containing missing data) and climate models (with variable numbers of days in calendar months), the YPS was estimated from monthly mean precipitation values. The number of dry days is larger than the number of wet days ($P_w \approx 0.26$), which may distort the calculation of observed monthly means, and lead to slight overestimation of observed

amounts of rain.

2.5. Spectral analysis

Generally, 2–7-year oscillations are attributed to ENSO, which is a globally dominant form of variability on annual to decadal time scales (e.g., Kleeman, 2008). It is a broadband phenomenon with several spectral peaks, the highest of which occurs at around 4 years. The 2013 IPCC report (Ch. 9.5, Flato et al., 2013) states that the representation of ENSO in the CMIP5 climate models has improved since CMIP3, and that most CMIP5 models express maximum variability at the observed time scale (2–7 years). However, errors persist in GCMs, such as in the amplitude, period and spatial patterns of ENSO.

To evaluate how the GCMs capture ENSO in the study region, and whether the bias correction has an effect on ENSO-related oscillatory patterns, the multitaper spectral analysis method (MTM, Thomson, 1982; Mann and Lees, 1996) was applied to calculate the spectra of the modeled time series at the observational station locations (Fig. 1, Table 1). MTM is appealing because it simultaneously reduces both the bias and error variance of spectral estimates (Babadi and Brown, 2014). It uses a small set of tapers instead of a unique data taper or spectral window, as are used in the classical methods for spectral estimation. The data are premultiplied by orthogonal tapers, which yield a set of independent estimates of the power spectrum. Finally, this ensemble of estimates is averaged to obtain an estimate of the power spectrum with lower variance (Ghil et al., 2002).

Monthly time series of temperature and precipitation were calculated for the stations presented in Table 1. Only the RCP4.5 runs were used in the MTM analysis. Before proceeding with MTM, the annual cycle was estimated using STL (Loess-based Seasonal-Trend Decomposition; Cleveland et al., 1990) and subtracted from the monthly time series. Otherwise, the annual cycle would dominate the spectral analysis results. The STL method is a filtering procedure for decomposing time series into trend, seasonal, and remainder components, and has been described in detail by Cleveland et al. (1990). The linear trends were also removed from the original and bias-corrected time series data.

The results of MTM analysis were scaled (i.e., the spectra of the original and bias-corrected data sets were divided by their standard deviations) to facilitate comparison of the original and bias-corrected data sets. Therefore, this analysis was focused on the locations and relative magnitude of the peaks before and after the bias correction. The intensity of the peaks was not compared in this study.

2.6. Hydrological model and modeling approaches

WEAP is a hydrological model developed at the Stockholm Environment Institute in Boston, Massachusetts, and is widely used for integrated water resources management. The model is based on the principle of water balance to represent the hydrological processes simulated in contributing catchments.

WEAP is a semi-distributed model, which means that the hydrological processes occurring in the sub-basins/tributaries of the main channel are represented in isolation. In addition, discharges at the intersections of tributaries are estimated (Fig. 1). The WEAP model applies different methods to simulate the internal processes of a watershed. In this study, the “Soil Moisture Model” method was selected, which is the most complete, for simulation of the processes of the hydrological cycle (Yates et al., 2005a,b). For hydrological simulation at monthly time steps, the model requires a number of different input variables, such as temperature, relative humidity, mean wind speed, latitude, precipitation, and vegetation coverage, from which the components of the hydrologic balance, such as evapotranspiration, infiltration, surface and subsurface runoff and baseflow, are estimated. The FAO Penman–Monteith equation (Allen et al., 1998) is used to calculate evapotranspiration based on the observed or estimated relative humidity and wind in the area.

To delineate the CH Basin into sub-basins using GIS (Geographic Information System) software, a numerical elevation model of the National Geographic Institute (IGN-Peru) at a scale 1:10,000 was employed. Each catchment unit of the WEAP model is divided into different classes of vegetation cover, and water balance is calculated for each class under an assumed uniform climate (Estebe et al., 2015). Five types of vegetation cover in the basin were defined: Puna grassland, high Andean land without vegetation, wetlands/reservoirs, thickets, and coastal plains. Vegetation cover information was compiled from the database of the *National Plan for Risk Management and Adaptation to the Adverse Effects of Climate Change on the Agricultural Sector* (PLANGRACC; PLANGRACC, 2012). The climatology for total monthly precipitation at the centroid of each catchment was determined using the Kriging interpolation method with the Hydraccess tool (Vauchel, 2005). For monthly temperature data, a monthly elevation–temperature equation was used, which is considered valid throughout the basin. For relative humidity and wind speed, monthly mean values were used, because continuous and reliable information for these variables is lacking. Agricultural and population water demand (PMGRH-II, 2012) was included in the hydrological model. A return flow of 30% was assumed for irrigation (water leaving the area of cultivation) and the cities in the middle and upper basin area.

Time series from the weather stations in neighboring watersheds, Huaura and Chillon, were used to replace missing values for some stations prior to hydrological modeling. The uncertainty of this gap filling procedure is considered minor, because (1) the data for modeling were replaced only for elevations over 2500 m above sea level, where seasonal temperature variation is small; (2) monthly data were used, and therefore the noise between neighboring stations is much smaller than that of the daily data (Rau et al., 2017); and (3) the neighboring watersheds belong to the same hydrological region as the study area. In addition, compared with temperature and precipitation, the contributions of relative humidity and wind speed are not significant in the simulation of flows; therefore, these variables were treated as fixed values for the control and scenario periods.

The WEAP model was calibrated using SENAMHI weather station and hydrological data based on comparing the observed and

simulated river flows for the period 1969–1978. The calibration was then validated using the period 1979–2012. The hydrological parameters that represent the rainfall–runoff processes are the crop coefficient (K_c), soil water capacity (S_w), deep water capacity (D_w), runoff resistance factor (RRF), root zone conductivity (K_s), deep zone conductivity (K_d), flow direction (f), and water stored in the root zone and the deep zone with respect to total storage capacity (Z_1; Z_2). Table 2 shows the calibrated parameter values used in the model. The accuracy of the model was measured using the Nash–Sutcliffe (E) efficiency coefficient, the coefficient of determination (R^2) and error rate (PBIAS). According to Moriasi et al. (2007), the attained E coefficients of 0.80 and 0.82; R^2 of 0.83 and 0.79, and the PBIAS of the model from −9% to −4%, for calibration and validation, respectively, represent a good level of accuracy.

3. Results and discussion

3.1. Temperature

Because of the coarse grid size, the GCMs failed to reproduce the large gradient in temperatures between the observational stations. The lack of inter-seasonal variation in the uncorrected GCMs compared with observed values was more prominent for the coastal station (Huayan) than for the inland stations (Canta, Picoy, Marcapomacocha). Therefore, larger adjustment was needed for the coastal area.

The ability of the uncorrected GCMs to produce the observed climate varied substantially within the basin (Fig. 2). The annual temperature cycle and small inter-seasonal variation of the inland stations (Picoy, Canta, Marcapomacocha) were, on average, well captured by the GCMs, although the monthly mean temperatures were overestimated throughout the year (monthly climatological root mean square error (RMSE): 0.7–23 °C). In contrast, monthly mean temperatures were closer to observed values at Huayan (monthly RMSE: 0.9–9.5 °C), but the GCMs failed to reproduce the observed annual cycle of temperature; either the seasonal cycle occurred in an altered phase or the inter-seasonal variation was insufficient (Fig. 2). The GCMs generally overestimated monthly mean temperatures throughout a year, with some exceptions, for the Huayan station on the coastline (Fig. 2). A majority of the GCMs simulated the seasonal minima of monthly mean temperatures one to two months ahead of observed cycle, and the maxima one month later than observed cycle (or during the wrong season) throughout the basin. The emission scenarios RCP4.5 and RCP8.5 did not differ in the control period 1981–2010, and therefore only the results for RCP4.5 are shown.

Bias correction reduced the systematic warm bias and adjusted the monthly mean temperatures toward the observed values in the control period (Fig. 2). The RMSE of the GCM-simulated monthly mean temperatures decreased to 0.4–1.5 °C for inland stations and to 0.9–2.5 °C at Huayan. We found the largest differences between the bias-corrected and observed monthly mean temperatures from May through June, which originated from the GCM-simulated phase offset of the seasonal cycle.

The GCM-simulated mean annual temperatures in the basin to increase by 1.0–4.8 °C under RCP4.5 (Fig. 3) and by 1.9–5.2 °C under RCP8.5 in 2051–2080 compared with the control period. The simulated increase was largest in the dry season (May–October) and smallest in the wet season (November–April) throughout the basin (Table 3). The increases in mean annual temperatures at the inland stations after bias correction, compared with the control period, were 1.1–5.0 °C under RCP4.5 and 1.7–5.9 °C under RCP8.5. The change after bias correction at the inland stations was generally small, and the trend indicated by GCMs can be regarded as preserved (Table 3). Bias correction altered the indicated warming by −1.6 °C to 1.3 °C (GCM ensemble mean: 0.4 °C) under RCP4.5 and by −1.5 °C to 1.3 °C (mean: 0.5 °C) under RCP8.5 compared with the uncorrected values.

Projection uncertainty is likely to be larger in the correction of the future period if the observed and modeled climates for the calibration period differ significantly. These differences distort the correction function as follows: (1) malformation of the shape of the histogram for the future period (upper panel in Fig. 4, where the distortion of the correction function leads to a bimodal distribution) and (2) changes in the mean climate change signal (lower panel in Fig. 4). The latter error (2) is particularly strong at Huayan, which is a coastal station and therefore suffers from dampened modeled variability. The quantiles in the correction function are tilted toward a vertical orientation, and the future climate is projected mainly based on the upper extrapolated tail of the correction function, which enhances the climate change signal. At Huayan, the bias correction altered the GCM-indicated temperature change substantially, by 0.3–2.5 °C (GCM ensemble mean: 1.5 °C) under RCP4.5 and by 0.4–2.7 °C (mean: 1.9 °C) under

Table 2
Hydrological parameters used in the WEAP model and their calibrated values. Definitions are given in the text.

Parameter	Value	Unit
K_c	0.7	–
S_w	200	mm
D_w	800	mm
RRF[a]	E = 5, H = 1.4	–
K_s[a]	E = 150, H = 600	mm/month
K_d	150	mm/month
f	0.5	–
Z_1	50	%
Z_2	50	%

[a] H = humid period, E = dry (low water level) period.

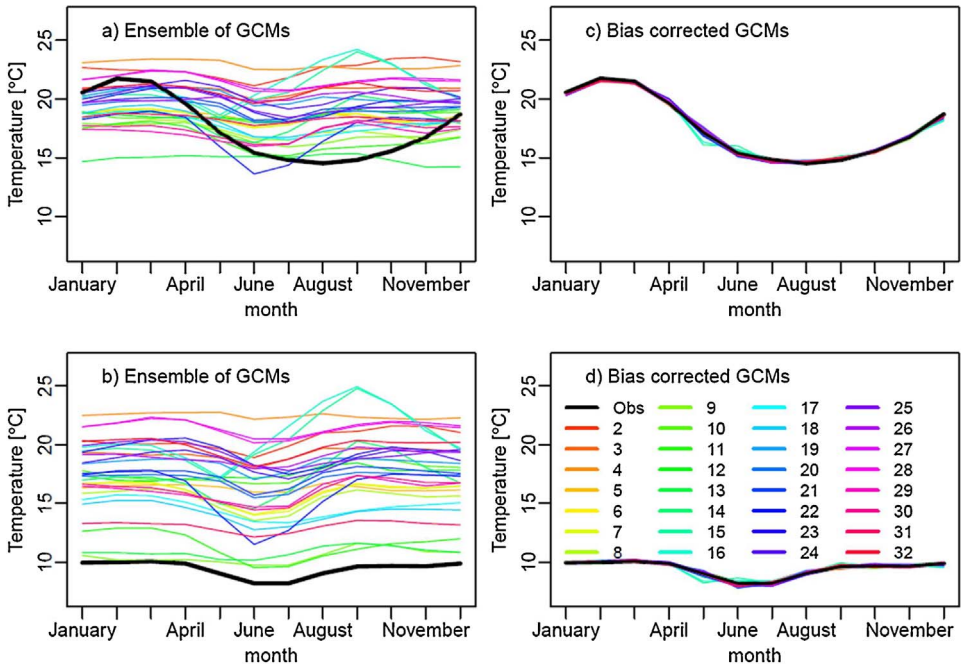

Fig. 2. Climatological monthly mean temperatures in Huayan (upper panels, a,c) and Picoy (lower panels, b,d) during the control period 1981–2010. Observations in black, GCMs in colors, numbered from 2 to 32. The numbering of the GCMs corresponds to the naming sequence in Fig. 6. The left column (a,b) illustrates the monthly mean temperatures before bias correction, and the right column (c,d) shows those after bias correction. Obs = observations.

RCP8.5.

3.2. Precipitation

The GCMs captured the seasonal cycle of precipitation, but the modeled daily and monthly mean accumulated totals were too high; the monthly RMSE of daily mean precipitation varied from 0.02 to 13.0 mm/day at the three stations (Carac, Pallac and Santa Cruz). The largest RMSE of the GCM data are found for January through March. Nonetheless, the greatest relative overestimation occurs in dry months (June–August, Table 4).

Based on comparison of the 1981–2010 multi-model mean spatial precipitation patterns of the GCMs to satellite observations (not shown), the likely reason for the overestimation of precipitation is apparent: the flattened orography of Andean region in the GCMs allows moisture to flow over the area toward the Pacific Ocean, which also extends the precipitation pattern southwest. How much this effect modifies climate change signals in the coastal region remains unclear. However, if the modeled rainfall pattern is shifted spatially such that it overlaps with the observed pattern (i.e., northeast), the signal of increasing mean precipitation weakens but remains positive in CH Basin (not shown).

The GCMs overestimate the number of wet days by simulating at least drizzle almost every day of the year. Excessive overestimation of drizzle, especially during the dry season (May–October), resulted in a greater error relative to observed values (Table 4, Fig. 5). In contrast, overestimation of total precipitation in summer is caused by too large amounts of daily precipitation. The frequency of wet days is critical information for the CH Basin, where the accessibility of freshwater resources during the arid season (May–October) relies on the accumulation of precipitation during the rainy season (November–April). The GCMs tend to overestimate the wet day frequency and reproduce too much drizzle in the basin, especially for the dry season. This overestimation is problematic for areas where the dry and wet seasons differ significantly.

Bias correction reduced the monthly RMSE of daily precipitation to 0.02–3.9 mm/day at the three stations (Carac, Pallac, and Santa Cruz). In addition, the large errors in accumulated precipitation during the arid winter season declined considerably (Table 4, Fig. 5). The effect of bias correction on changes in precipitation did not vary spatially as with temperature. However, no precipitation stations were available near the coastline.

Most of the GCMs simulated increased total annual precipitation for the basin for the future period (2051–2080) compared with the control period (Fig. 3, Table 4). Seasonal change of accumulated precipitation compared with GCM values in the control period varied from −294 mm/season to +323 mm/season (GCM ensemble mean: 31 mm/season) under RCP4.5 and −278 mm/season to +421 mm/season (mean: 40 mm/season) under RCP8.5. Absolute amounts of precipitation are expected to increase most in the wet season. Bias correction dampened the expected change to −60–177 mm/season (mean: 23 mm/season) under RCP4.5 and to −75–227 mm/season (mean: 32 mm/season) under RCP8.5 at the three stations, compared with bias-corrected values for the control period. Bias correction affected precipitation amounts most during the dry season, which was expected based on the large overestimations of the GCMs for this season.

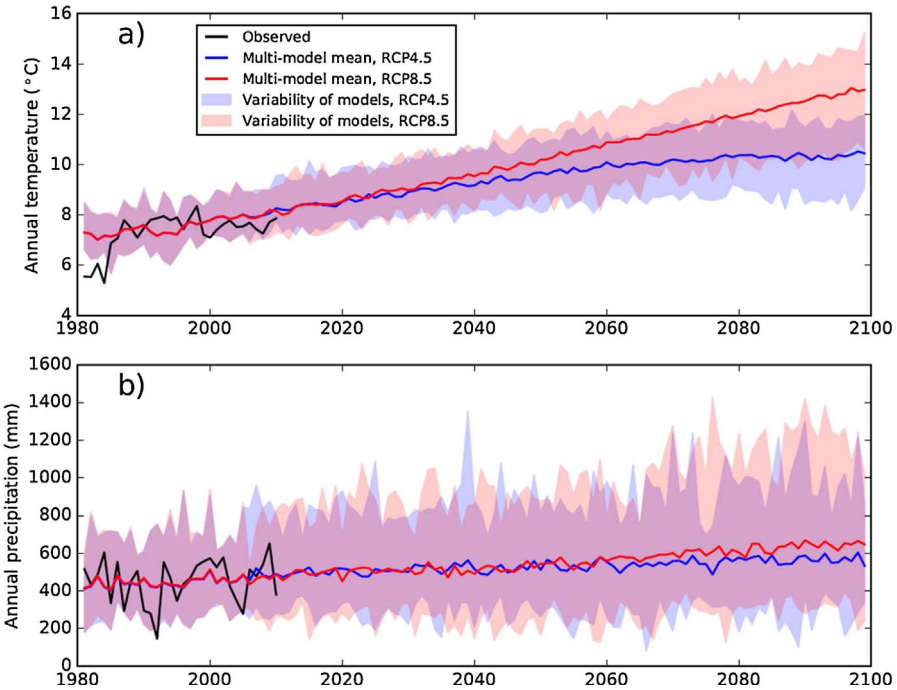

Fig. 3. (a) Annual mean temperature and (b) annual precipitation totals (1981–2099) for selected stations of the Chancay-Huaral Basin. Temperature means were calculated as averages over Picoy, Canta, and Marcapoma, and precipitation sums as averages over Carac, Pallac and Santa Cruz. Observations shown in black, bias-corrected GCMs driven with the emission scenario RCP4.5 in blue and those with RCP8.5 in red. GCM ensemble mean values are shown with solid lines, and ensemble variation with transparent highlighted areas. (For interpretation of the references to colour in this figure legend, the reader is referred to the web version of this article.)

Table 3
Seasonal mean temperatures of observations (Obs), unadjusted projections (GCMs) and bias-corrected GCM (BC) projections as ensemble mean values for the Canta station. Results are shown for the control (1981–2010) and scenario (2051–2080) periods under emission scenario RCP4.5. In addition, the results for RCP8.5 are shown for the scenario period. Table illustrates GCM ensemble mean values for seasonal mean temperature (°C). Annual averages (ANN) are shown in the bottom row.

Season	1981–2010			2051–2080			
	Obs	GCM	BC	GCM		BC	
		RCP4.5	RCP4.5	RCP4.5	RCP8.5	RCP4.5	RCP8.5
DJF	11.1	17.8	11.1	19.6	20.5	13.4	14.3
MAM	11.2	17.5	11.3	19.5	20.5	13.5	14.5
JJA	11.0	16.8	11.0	19.0	20.1	13.5	14.7
SON	11.3	18.0	11.4	20.1	21.2	13.8	15.0
ANN	11.2	17.5	11.2	19.5	20.6	13.6	14.6

DJF = December–February, MAM = March–May, JJA = June–August, SON = September–November, ANN = January–December.

On average, the frequency of wet days will increase only slightly toward the end of this century under both RCP4.5 and RCP8.5 (Table 4, Fig. 6). RCP4.5 and RCP8.5 produce similar patterns in wet day frequency, but RCP8.5 simulates daily precipitation amounts up to 41% larger than those produced under RCP4.5.

3.3. Precipitation indices

The quantile mapping bias correction method adjusts the mean values and the shape of the distribution, but does not modify the chronological structure of the time series. Therefore, statistics that measure the temporal aspects of data distributions are useful for validating the performance of individual GCMs. For example, the SPI index is affected by the temporal characteristics of the precipitation time series, and models with distribution of SPI values that are too narrow or too wide are more questionable than models with SPI distributions more similar to observations. Because the analysis is mostly based on values of individual grid cells, the overall or regional performance of the models cannot be seen, but local validation is valuable. Similarly, the 30-year distributions of annually aggregated values of YWD and YPS can be regarded as a validation metric that describes the ability of the models to reproduce local interannual variability.

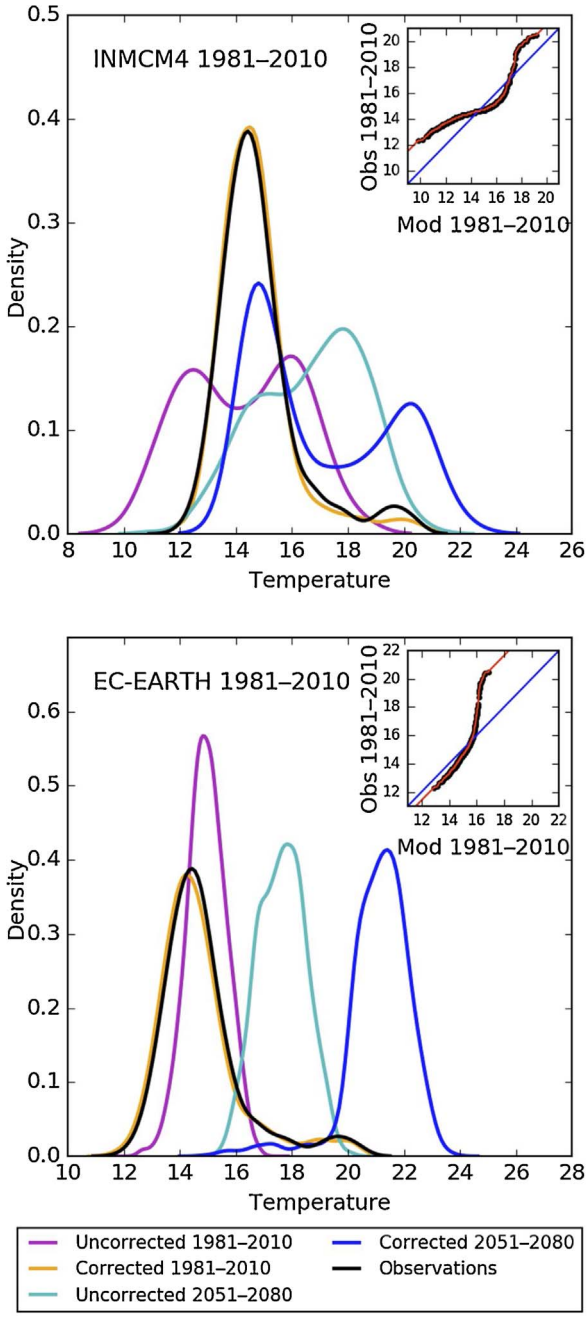

Fig. 4. Typical problems in temperature correction at coastal stations: malformation of the future temperature histogram (upper panel, INMCM4 model) and transformation of the climate change signal (lower panel, EC-EARTH model) with July temperatures in Huayan. Small inset panels show the quantiles (black dots) and the corresponding correction functions, including the linearly extrapolated parts (red). See text (Section 3.1) for explanations. (For interpretation of the references to colour in this figure legend, the reader is referred to the web version of this article.)

As shown in Fig. 6, the median, 25% and 75% values, and the tails of the SPI-6 precipitation index in the control period are relatively well captured by the corrected climate models on average. However, the dry tail is generally overestimated: only two models reach wet-season SPI values of −2 ('extremely dry'; WMO, 2012) in 1981–2010, even though this value has been observed twice, in 1990 and in 1992. Three models project the mean SPI-6 value exceeding 2 in 2051–2080, but generally, the mean future SPI-6 is projected to be between 0.5 and 1.5, with a mean change of +0.8. Of the 31 models, 17 show statistically significant (*t*-test, $P < 0.05$) increases in the SPI-6 index. Three models show decreasing signals. Long-duration wet (dry) periods increase (decrease) the SPI value, but the amount of precipitation also affects this index. As shown in Table 3, the length of the wet season in days is not expected to change remarkably. Instead, the amount of precipitation is projected to increase, which explains most of the projected

Table 4
Seasonal precipitation characteristics of observations (Obs), unadjusted projections (GCMs) and bias-corrected GCM projections (BC), as GCM ensemble mean values for the Santa Cruz station. Results are shown for the control (1981–2010) and scenario (2051–2080) periods under emission scenario RCP4.5. In addition, the results for RCP8.5 are shown for the scenario period. GCM ensemble mean values for seasonal precipitation totals (Total), are given in mm, and the number of wet days (Days) as the mean seasonal number of wet days during the study period. Annual averages (ANN) are shown in the bottom two rows.

Season		1981–2010			2051–2080			
		Obs	GCM	BC	GCM		BC	
			RCP4.5	RCP4.5	RCP4.5	RCP8.5	RCP4.5	RCP8.5
DJF	Total	283	725	310	784	797	364	379
	Days	49	90	55	90	90	57	57
MAM	Total	186	530	198	570	588	230	245
	Days	37	91	39	91	91	41	40
JJA	Total	6	71	6	78	71	8	9
	Days	3	87	3	86	86	3	3
SON	Total	98	434	113	455	459	135	145
	Days	23	90	26	90	90	28	29
ANN	Total	573	1759	627	1887	1916	738	779
	Days	112	359	123	358	358	129	129

DJF = December–February, MAM = March–May, JJA = June–August, SON = September–November, ANN = January–December.

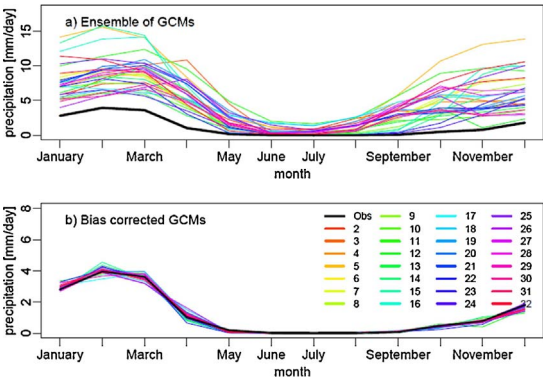

Fig. 5. Daily mean precipitation totals in Carac during the control period 1981–2010. Observations (Obs) in black, GCMs driven with emission scenario RCP4.5 in colors, numbered from 2 to 32. The numbering of the GCMs corresponds the naming sequence in Fig. 6. Upper panel illustrates the daily mean precipitation totals before bias correction, and the bottom panel those after bias correction.

positive change in the wet season SPI-6 index.

The two other precipitation indices show qualitatively similar performance and climate change signals in the different climate models: both show change toward wetter conditions. Some models indicate particularly strong climate change in the wet tail of the YPS index, with one model showing maximum precipitation of 1400 mm/year. The quantile mapping procedure enhances the extreme values of daily precipitation in the tails of the distributions when corrected data from several stations are combined (Maraun, 2013), and it is possible that this effect can still be seen in the results, even after monthly averaging of the time series.

The observed variability of the YWD in tails of the distribution is not fully covered by most of the climate models. The 25–75% range and median are generally better represented. Because the amount of precipitation and the number of dry days are not projected to change in the dry season (Table 4), the climate change signal comes mainly from the wet season.

3.4. Effect of bias correction on oscillatory behavior of ENSO

The results of the MTM analysis were scaled (i.e., the spectra of the original and bias-corrected data sets were divided by their standard deviations) to facilitate comparison of the original and bias-corrected data sets. Therefore this analysis was focused on the locations and relative magnitudes of the peaks before and after bias correction. The intensity of the peaks was not compared herein.

The MTM analysis reveals that the oscillatory behavior related to ENSO is essentially preserved after bias correction. In particular, the spectra of the temperature time series show good agreement between the original and bias-corrected data. The spectra of the precipitation time series show greater difference in the locations (and shapes) of the peaks, but 2–7-year oscillations are generally preserved. However, the 2–7-year peaks are more clearly distinguishable in the temperature data sets compared with the precipitation data sets, which show more randomness in their spectra. The statistical significance of the peaks was not studied here because the qualitative estimation of the ENSO preservation after the bias correction is sufficient at this point. The spectra of the original and bias-corrected temperature data sets are shown for the models MPI-ESM-MR and EC-EARTH and the Picoy, Canta, and

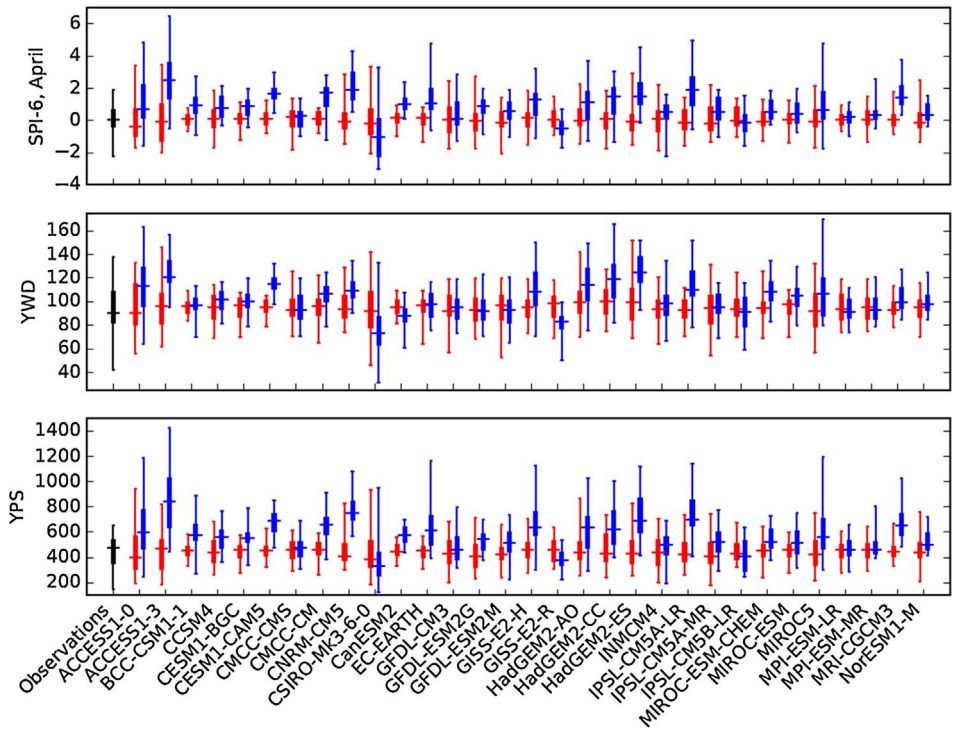

Fig. 6. Variability of precipitation indices (SPI-6 = six-monthly standardized precipitation index, YWD = yearly number of wet days, YPS = yearly precipitation sum in millimeters) calculated as means over the three precipitation stations (Carac, Pallac and Santa Cruz). For SPI-6 the values for the wet season (November–April) months are shown. Black: observations from 1981 to 2010. Red: corrected climate models for 1981–2010. Blue: corrected climate models for 2051–2080 (RCP8.5). Whiskers indicate the absolute minimum and maximum values during the corresponding period; 25%, 75% and 50% values are shown respectively by the box edges and horizontal lines. The naming sequence corresponds the numbering of the GCMs in Figs. 2 and 5 (number 1 being observations).

Huayan stations in Fig. 7.

ENSO affects seasonal climatic variability in this area, and may cause strong floods and droughts. The CH Basin is located in area where the impacts of ENSO can vary greatly over short distances (Lavado-Casimiro et al., 2013). The southern and northern parts of the Peruvian coastline may undergo opposite impacts (floods/droughts) during El Niño and La Nina, and therefore the specific signal in the CH Basin remains uncertain.

Kim and Yu (2012) found that the simulated intensity of Eastern Pacific ENSO decreases toward the end of 21 st century. This trend was also apparent in our temperature time series (not shown). Our goal was only to detect if the bias correction alters the ENSO

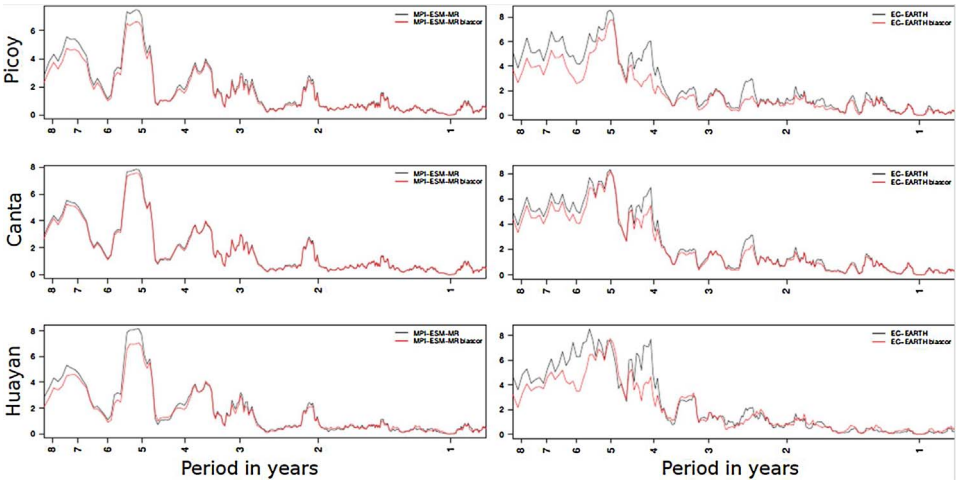

Fig. 7. The spectra of the original (black lines) and bias-corrected (red lines) monthly mean temperature data sets (calculated over the period 1970–2100) for the models MPI-ESM-MR and EC-EARTH and for the stations Picoy, Canta, and Huayan. (For interpretation of the references to colour in this figure legend, the reader is referred to the web version of this article.)

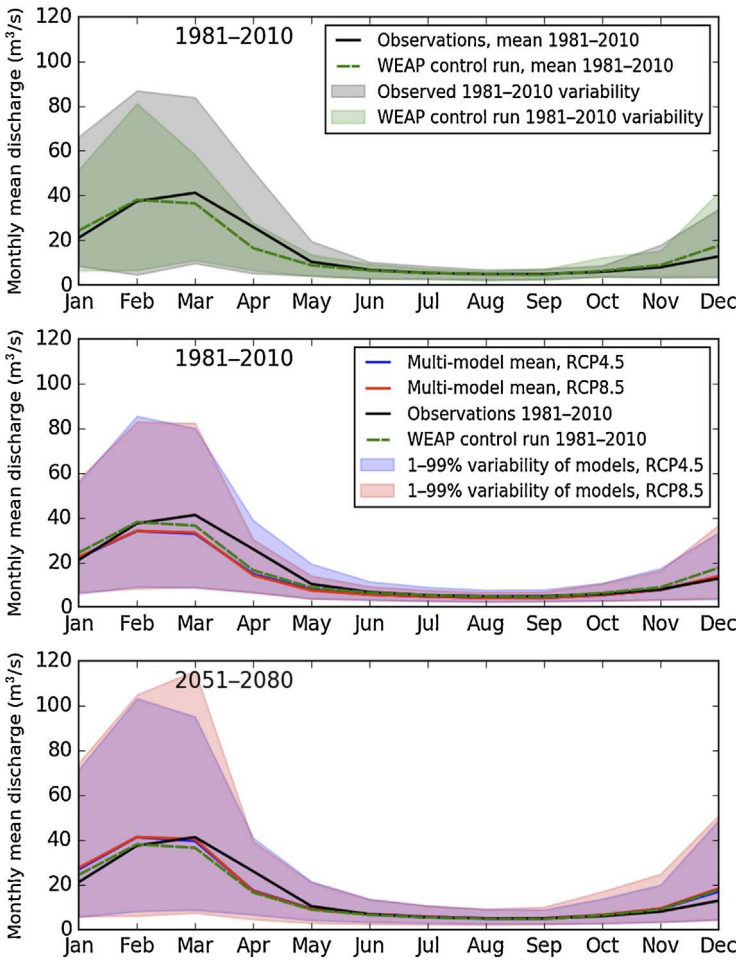

Fig. 8. Monthly mean discharges in observations (1981–2010, upper panel) and as simulated with GCMs for the control (1981–2010, middle panel) and future (2051–2080, lower panel) periods. Observed discharges are shown as black solid lines, discharges simulated based on observed temperature and precipitation data with the WEAP model as dashed green lines, GCM ensemble mean values under RCP4.5 as solid blue lines, and those under RCP8.5 as solid red lines. Variation (1–99% range) is shown as transparent highlighting with the corresponding colors. (For interpretation of the references to colour in this figure legend, the reader is referred to the web version of this article.)

cycle, not to study the effects of ENSO or the possible changes to ENSO caused by climate change by ENSO. The data set was constructed from a limited selection of ground-based stations within a small basin, which is not a sufficiently broad and reliable source to reconstruct ENSO cycles.

3.5. Discharges

The WEAP model simulates the observed seasonal cycle of river discharge reasonably well (Fig. 8, top panel), but tends to underestimate observed discharges in wet periods, especially during peak flows. Therefore, the largest biases can be found for discharge in the wet season. The simulated overestimated discharge values in wet periods (mainly in December) and too-early decreases in discharge from March to May are caused in part by the low density of observational stations for information related to the rainfall–runoff relationship in the upper parts of the basin, and in part by the deficiencies in modeling the tributaries and reservoirs that restore the water masses and delay the maximum discharges by a month or more. As stated in Section 2.6, information about the sub-basins and tributaries in this basin is scarce or unavailable. In addition, the groundwater in the CH River Valley is exploited in various ways. Natural underground springs, vital in low-water years, are the primary source of irrigation, with an annual supply of about 80–100 MMC, entirely from seepage of irrigation water. These springs may be permanent or temporary, and may provide up to 30% of the water used in irrigation in years with low availability of surface water. This water is itself composed of return water, natural funnels, and groundwater drains recovered through open pits.

As recent improvements, new hydrological stations have been implemented in the CH Basin through the Modernization of Water Resources Management Project (*Proyecto Modernización de la Gestión Integrada de los Recursos Hídricos*), which in the short term will enable collection of information, and in the future will improve discharge estimates by adjusting model parameters.

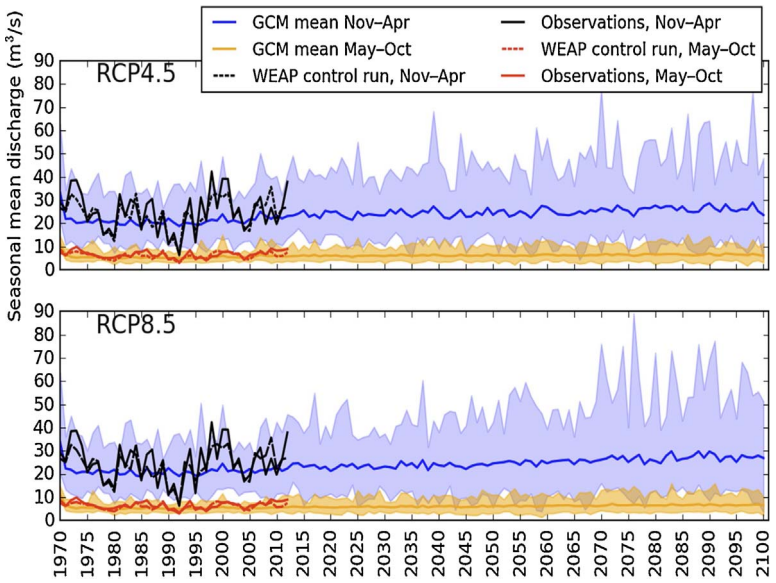

Fig. 9. Seasonal mean discharges (m^3/s) in observations (1981–2010, black and red solid lines), in the WEAP control run (black and red dashed lines), and as simulated with 31 GCMs (1981–2099) for the dry and wet seasons, with RCP4.5 in the upper panel and RCP8.5 in lower panel. GCM ensemble mean values for November–April (wet season) are shown with blue solid lines and for May–October (dry season) with orange solid lines. Total variation between GCMs is shown as transparent highlighting with the corresponding colors. (For interpretation of the references to colour in this figure legend, the reader is referred to the web version of this article.)

Bias correction was performed for the temperature and precipitation values from all 31 GCMs prior the generation of discharge scenarios to avoid unnecessarily large uncertainty ranges and false conclusions about the impacts of climate change. The mean monthly cycle of discharge simulated with bias-corrected values from the GCMs is close to observed values, but the values are systematically underestimated (Fig. 8, central panel). Nevertheless, the observed (WEAP control run) variability of the wet and dry seasons is captured by the model ensemble (Fig. 9).

In addition, most of the WEAP simulations with GCM forcings (68% of the GCMs) were able to reproduce annual mean discharges below 8 m^3/s (which corresponds to the 5th observed percentile) in the control period. This result is encouraging because accurate simulation of the low end of discharge distribution is essential for the study of droughts. In contrast, only 26% of the GCMs reproduced the extreme high flows of $Q > 23$ m^3/s (95th observed percentile). GCMs that simulated low flows more frequently relative to other GCMs also simulated high flows more frequently; 23% of the GCMs yielded both extreme values, and 71% simulated at least one extreme.

GCM simulations indicate that the magnitude of mean monthly discharge would increase in all months by 17% (August) to 31% (December) on average, from the control period to 2051–2080 (Fig. 8, middle and lower panels). These results are nearly independent of the emission scenario used. In absolute units, the multi-model ensemble means show increases in discharge between 0.7 m^3/s (August) and 7.2 m^3/s (February). The projected annual increases are 20% and 22% under RCP4.5 and RCP8.5, respectively. The differences in annual means between RCP4.5 and RCP8.5 are small ($\pm$ 2.5 m^3/s), and the multi-model mean values overlap even at the end of the century (not shown). The proportion of models showing mean annual discharge values below 8 m^3/s decreases from 68% to 26% in the future period. This result is independent of the emission scenario used. However, 45% (RCP4.5) and 48% (RCP8.5) of the GCMs show mean annual discharges above 23 m^3/s in the future. The percentage of models in which both extreme values are exceeded decreases to 13% (RCP8.5) and 16% (RCP4.5), mostly because of decrease in the number of values below 8 m^3/s. Similarly, 55% (RCP4.5) and 61% (RCP8.5) of the models yield discharge values that exceed at least one of the extremes.

Discharge amounts are expected to increase throughout a year, but as the increases in precipitation amounts imply, the increase in discharge is larger in the wet season (November–April) than in the dry season (May–October). The GCM ensemble mean discharge increases by 17% and 20% under RCP4.5, and by 20% and 22% under RCP8.5, in the dry and wet seasons, respectively, from the control period to 2051–2080 (Fig. 9). In addition, the variability increases toward the end of the century as the highest annual discharges more frequently shows higher values than those simulated in the control period, and the lower discharge amounts, although scant, become even lower. These findings indicate that even though the mean values increase with time, arid years may become even more arid.

3.6. Comparison with earlier research

Similar to the CMIP5 GCM projections of climate change used in this study, earlier-generation GCMs projected temperature increases over the Peruvian region toward the latter part of 21st century (e.g., see the IPCC AR5 (IPCC, 2013) compared with the IPCC AR4 (Christensen et al., 2007)). Furthermore, the downscaled temperature projections preserve the warming trend (Marengo et al.,

2010; Franchito et al., 2014; MINAM, 2016). Bias-corrected temperature projections presented in this study thus agree well with earlier research.

GCM projections of precipitation changes continue to display both increasing and decreasing trends over Pacific coastal regions of Peru. The IPCC AR4 GCM ensemble mean projected precipitation increase; however, 1–4 models out of 21 indicated a decrease in annual mean precipitation over coastal Peru in the future. The IPCC AR5 GCM ensemble mean shows positive trends in the amounts of precipitation in both the wet and dry seasons under the RCP4.5 scenario in Peruvian coastal regions from the period of 1986–2005 to 2046–2065 (IPCC, 2013). However, the corresponding lower 25th percentile maps show patchy features of precipitation change where drying dominates along the Peruvian coast in both the wet and dry seasons. The bias correction we applied dampened both increasing and decreasing seasonal precipitation trends of GCMs in the CH Basin. In general, our study gives qualitatively similar result to those of the IPCC (2013) for the Peruvian coastal region; i.e., the ensemble mean precipitation increases, but some of the GCMs project decreasing trends.

Earlier studies that utilized both dynamically and statistically downscaled GCM projections of precipitation showed mixed results in the Lima Region, which includes the CH Basin (Buytaert et al., 2010; Marengo et al., 2010; Kitoh et al., 2011; MINAM, 2016). Regional climate models capture local gradients, but are still prone to large discrepancies between observed and modeled precipitation. Buytaert et al. (2010) concluded that a further increase in resolution is necessary to properly represent local gradients. It is also important to note that the mean projected precipitation changes in the study region are consistent with those of the IPCC (2013) within less than the standard deviation of the model-estimated present-day natural variability of the 20-year mean differences until the mid–21 st century.

The simulated discharges for the multi-model mean in the CH Basin based on bias-corrected and downscaled GCM projections increase most during the wet season, which is in accordance with the simulated larger increase in precipitation during that season. The mean multi-model discharge increase is only slightly larger under the RCP8.5 scenario than under the RCP4.5 scenario, likely because the larger increases in temperature and evaporation reduce the impact of increased precipitation under RCP8.5. The simulated changes in discharge range from slightly negative to clearly positive trends. In the Lima Region, earlier studies of runoff, aridity and discharge based on downscaled climate change simulations show mixed results with increasing and decreasing discharges, as expected based on the corresponding precipitation changes (Marengo et al., 2010; Franchito et al., 2014; MINAM, 2016).

4. Conclusions

The hydrological situation in Peru can be characterized as one with severe spatial imbalances between supply (in the Andes) and demand (in the heavily populated coastal zone) and with mounting challenges caused by rapid changes in demographics and land use in the coastal zone. Because water and climate change are highly relevant concerns for sectors such as agriculture, projections of water resources under climate change have become an important element for national and regional planning.

The Pacific coastal region is characterized by relatively narrow but steep slopes, and therefore, peaks in rainfall and the associated discharge can occur nearly simultaneously without reservoirs to detain water masses. The simulated annual maximum flow in the CH Basin occurs in February, when the maximum precipitation also occurs, whereas in observations, the maximum discharge occurs one month later. This error in timing is likely the result of the incomplete representation of tributaries and reservoirs, which may delay the observed timing of maximum discharge. Despite the lack of water use information for the WEAP, the model can simulate the observed discharges relatively well.

Discharge scenarios for the CH area were generated using bias-corrected temperature and precipitation values from 31 GCMs (RCP4.5 and RCP8.5). Bias correction preserves the climate change signal of GCMs relatively well, except in the coastal area. Because the WEAP hydrological model uses monthly mean values and integrates temperature and precipitation data from several stations, the uncertainties related to the quantile mapping bias correction method are reduced in the flow results. Annual mean temperature and precipitation are expected to increase in the CH Basin in 2051–2080 compared with the control period. Most of the climate models show statistically significant increases in the YPS and SPI-6 indices toward 2051–2080, and half show increases in the YWD index. The differences in precipitation between the RCP4.5 and RCP8.5 scenarios are rather small, and inter-model variability in precipitation is large, but in terms of temperature projections, the differences between the two scenarios are more distinct and the model outputs more consistent toward the end of this century.

Because total precipitation increases most during the wet season, discharge also increases most during that season. Temperature-dependent changes in evapotranspiration and precipitation have a tendency to partly offset each other making wet season discharge increases fairly insensitive to the emission scenario employed. Climate change affects the annual variability of precipitation, but ENSO and changes in water use are expected to remain the primary causes of drought in this region. Our results suggest that because the amount of precipitation is projected to increase, an increase of the storage of water during the wet season is one possible solution to improve water management options and alleviate water supply shortages during the dry season. However, there is considerable variation in the CMIP5 projections of climate change in the study area. Therefore, any near-term investment decisions on water security and quality will be done under substantial uncertainty regarding future river discharges. Thus, the current level of knowledge based on this study and earlier research reviewed suggests that water managers should apply rather robust than optimal decision-making approach where e.g. no-regret, low-regret options as well as flexible solutions are identified both in supply and demand of water resources.

Acknowledgments

This work was supported by the Finnish Academy through funding of the AquaFutura project (grant decision 250529) and by the Fortum Foundation (grant number 201500127). We acknowledge the World Climate Research Programme's Working Group on Coupled Modelling, which is responsible for CMIP, and we thank the climate modeling groups for producing and making available their model output. The U.S. Department of Energy's Program for Climate Model Diagnosis and Intercomparison provided coordinating support and led the development of software infrastructure in partnership with the Global Organization for Earth System Science Portals. We thank the editor, Professor Patrick Willems, and four anonymous reviewers for providing valuable comments to improve considerably the manuscript.

References

Allen, R.G., Pereira, L.S., Raes, D., Smith, M., 1998. Crop Evapotranspiration. Guidelines for Computing CropWater Requirements. FAO Irrigation and Drainage Paper No. 56. FAO (Food and Agriculture Organization of the United Nations), Rome, Italy.

ANA, 2011. Autoridad Nacional del Agua. Evaluación de los recursos hídricos superficiales en la cuenca del río Chancay-Huaral. http://www.ana.gob.pe:8094/media/38323/02.01%20erh_huaral2011_texto.pdf. (Accessed 11 Aug 2016).

Andréasson, J., Bergström, S., Carlsson, B., Graham, L., Lindström, G., 2004. Hydrological change −climate change impact simulations for Sweden. Ambio 33, 228–234.

Babadi, B., Brown, E.N., 2014. A review of multitaper spectral analysis. IEEE Trans. Biomed. Eng. 61 (5), 1555–1564. http://dx.doi.org/10.1109/tbme.2014.2311996.

Bates, B.C., Kundzewicz, Z.W., Wu, S., Palutikof, J.P. (Eds.), 2008. Climate Change and Water Technical Paper of the Intergovernmental Panel on Climate Change. IPCC Secretariat, Geneva (210 pp).

Buytaert, W., Vuille, M., Dewulf, A., Urrutia, R., Karmalkar, A., Celleri, R., 2010. Uncertainties in climate change projections and regional downscaling in the tropical Andes: implications for water resources management. Hydrol. Earth Syst. Sci. 14, 1247–1258.

Christensen, J.H., Krishna Kumar, K., Aldrian, E., An, S.-I., Cavalcanti, I.F.A., de Castro, M., Dong, W., Goswami, P., Hall, A., Kanyanga, J.K., Kitoh, A., Kossin, J., Lau, N.-C., Renwick, J., Stephenson, D.P., Xie, S.-P., Zhou, T., 2013. Climate phenomena and their relevance for future regional climate change. In: Stocker, T.F., Qin, D., Plattner, G.-K., Tignor, M., Allen, S.K., Boschung, J., Nauels, A., Xia, Y., Bex, V., Midgley, P.M. (Eds.), Climate Change 2013: The Physical Science Basis. Contribution of Working Group I to the Fifth Assessment Report of the Intergovernmental Panel on Climate Change. Cambridge University Press, Cambridge, United Kingdom and New York, NY USA.

Cleveland, R.b., Cleveland, W.S., McRae, J.E., Terpenning, I., 1990. STL: a seasonal-trend decomposition procedure based on loess. J. Off. Stat. 6, 3–73.

Espinoza, J., Ronchail, C.J., Guyot, J.L., Junquas, C., Vauchel, P., Lavado, W., Drapeau, G., Pombosa, R., 2011. Climate variability and extreme drought in the upper Solimões River (western Amazon Basin): Understanding the exceptional 2010 drought. Geophys. Res. Lett. 38, L13406. http://dx.doi.org/10.1029/2011GL047862.

FAO, 2013. FAO Statistical Yearbook 2013. World Food and Agriculture. http://www.fao.org/docrep/018/i3107e/i3107e00. htm. (Accessed 10 May 2017).

Flato, G., Marotzke, J., Abiodun, B., Braconnot, P., Chou, S.C., Collins, W., Cox, P., Driouech, F., Emori, S., Eyring, V., Forest, C., Gleckler, P., Guilyardi, E., Jakob, C., Kattsov, V., Reason, C., Rummukainen, M., 2013. Evaluation of climate models. In: Stocker, T.F., Qin, D., Plattner, G.-K., Tignor, M., Allen, S.K., Boschung, J., Nauels, A., Xia, Y., Bex, V., Midgley, P.M. (Eds.), Climate Change 2013: The Physical Science Basis. Contribution of Working Group I to the Fifth Assessment Report of the Intergovernmental Panel on Climate Change. Cambridge University Press, Cambridge, United Kingdom and New York, NY USA. http://dx.doi.org/10.1017/CBO9781107415324.020. (Chapter 9).

Franchito, S., Fernandez, J., Pareja, D., 2014. Surrogate climate change scenario and projections with a regional climate model: impact on the aridity in South America. Am. J. Clim. Change 3, 474–489. http://dx.doi.org/10.4236/ajcc.2014.35041.

Garreaud, R.D., Vuille, M., Compagnucci, R., Marengo, J., 2009. Present-day South American climate. Palaeogeography palaeoclimatology. Palaeoecology 281, 180–195.

Ghil, M., Allen, M.R., Dettinger, M.D., Ide, K., Kondrashov, D., Mann, M.E., Robertson, A.W., Saunders, A., Tian, Y., Varadi, F., Yiou, P., 2002. Advanced spectral methods for climatic time series. Reviews of geophysics 40 (1), 1003. http://dx.doi.org/10.1029/2000RG000092.

Haavisto, R., Santos-Villar, D., Perrels, A., Unpublished results: Determining payments for watershed services by hydro-economic modeling in the context of local water resource management, submitted to Water Resources and Economics in July 2017.

Hanssen-Bauer, I., Achberger, C., Benestad, R.E., Chen, D., Førland, E.J., 2005. Statistical downscaling of climate scenarios over Scandinavia. Climate Res. 29 (3).

IPCC, 2013. Climate change 2013: the physical science basis. In: Stocker, T.F., Qin, D., Plattner, G.-K., Tignor, M., Allen, S.K., Boschung, J., Nauels, A., Xia, Y., Bex, V., Midgley, P.M. (Eds.), Contribution of Working Group I to the Fifth Assessment Report of the Intergovernmental Panel on Climate Change. Cambridge University Press, Cambridge, United Kingdom and New York, NY, USA. http://dx.doi.org/10.1017/CBO9781107415324. (1535 pp)Kim, S.T., Yu, J.-Y., 2012. The two types of ENSO in CMIP5 models. Geophys. Res. Lett. 39, L11704. http://dx.doi.org/10.1029/2012GL052006.

Kitoh, A., Kusunoki, S., Nakaegawa, T., 2011. Climate change projections over South America in the late twenty-first century with the 20-km and 60-km mesh MRI-AGCM. J. Geophys. Res. 116, D06105. http://dx.doi.org/10.1029/2010JD014920.

Kleeman, R., 2008. Stochastic theories for the irregularity of ENSO. Philos. Trans. Roy. Soc. A Math. Phys. Eng Sci. 366 (1875), 2509–2524.

Lausent-Herrera, I., 1994. Impacto de las sequías en las comunidades de alto valle de Chancay 1940–1973. Bulletin de l'Institut Francais d'Etudes Andines, Tome 23, No. 1. pp. 151–170.

Lavado-Casimiro, W.S., Felipe, O., Silvestre, E., Bourrel, L., 2013. ENSO impact on hydrology in Peru. Adv. Geosci. 11 (1–7), 2013. http://dx.doi.org/10.5194/adgeo-11-1-2013.

Mann, M.E., Lees, J.M., 1996. Robust estimation of background noise and signal detection in climatic time series. Clim. Change 33, 409–445.

Maraun, D., 2013. Bias correction, quantile mapping, and downscaling: revisiting the inflation issue. J. Climate 26, 2137–2143. http://dx.doi.org/10.1175/JCLI-D-12-00821.1.

Marengo, J.A., 1995. Variations and change in South American streamflow. Clim. Change 31, 99–117.

Marengo, J.A., Tomasella, J., Uvo, C.R., 1998. Trends in streamflow and rainfall in tropical South America: Amazonia, eastern Brazil, and northwestern Peru. J. Geophys. Res. 103, 1775–1784.

Marengo, J.A., Ambrizzi, T., da Rocha, R.P., Alves, M.L., Cuadra, S.V., Valverde, M.C., Torres, R.R., Santos, D.C., Ferraz, S.E.T., 2010. Future change of climate in South America in the late twenty-first century: intercomparison of scenarios from three regional climate models. Clim. Dyn. 35, 1073–1097. http://dx.doi.org/10.1007/s00382-009-0721-6.

MINAG, 2002. Estrategia Nacional Forestal. Version concertada con instituciones y actores forestales. Ministerio de Agricultura, Lima, Peru.

MINAG, 2011. Estudio de Preinversion a Nivel del Perfil del Subcomponente C2: Sensibilization, Difusion y Asistencia Technica en Agricultura de Riego a Agricultores en la Junga de Usuarios de Colca Chivay Programa PSI −Sierra. Ministerio de Aqricultura, Arequipa, Peru.

MINAM, 2016. Tercera Comunicación Nacional del Perú ante la Convención de las Naciones Unidas sobre Cambio Climático. MINAM, Lima Peru (326 pp.).

McKee, T., Doesken, N., Kleist, J., 1993. The relationship of drought frequency and duration to time scales. In: Eighth Conference on Applied Climatology. 17-22 January 1993, Anaheim California.

Moriasi, D.N., et al., 2007. Model evaluation guidelines for systematic quantification of accuracy in watershed simulations. Trans. ASABE 50, 885–900. http://dx.doi.org/10.13031/2013.23153.

ONERN, 1969: Inventario, Evaluación y Uso Racional de los Recursos Naturales de la Costa: Valle Chancay-Huaral. 2 Vols., Lima.

PLANGRACC, 2012. Plan de Gestión de Riesgos y Adaptación al Cambio Climático en el sector Agrario. http://www.minagri.gob.pe/portal/plangracc. (Accessed 10 May 2017).
PMGRH-I, 2012: Tomo I. Proyecto de modernización de la gestión de los recursos hídricos −Diagnóstico participativo consolidado cuenca Chancay-Huaral. Aspectos generales, marco normativo e institucional y descripción de la cuenca. siar.minam.gob.pe/lima/download/file/fid/55199. (Accessed 10 May 2017).
PMGRH-II, 2012: Tomo II. Proyecto de modernización de la gestión de los recursos hídricos −Diagnostico participativo consolidado cuenca Chancay-Huaral. Situación actual de la gestión de los recursos hídricos. siar.minam.gob.pe/lima/download/file/fid/55200. (Accessed 10 May 2017).
PRB, 2010. Population Reference Bureau. http://www.prb.org/countries/peru.aspx. (Accessed 10 May 2017).
PROFODUA, 2005. Propuesta de asignaciones de agua en bloque (volúmenes anuales y mensuales) para la formalización de los derechos de uso de agua Chancay −Huaral del programa de formalización de derechos de uso de agua.
Rau, P., Bourrel, L., Labat, D., Melo, P., Dewitte, B., Frappart, F., Lavado, W., Felipe, O., 2017. Regionalization of rainfall over the Peruvian Pacific slope and coast. Int. J. Climatol. 37, 143–158. http://dx.doi.org/10.1002/joc.4693.
Romero, C.C., Baigorria, G.A., Stroosnijder, L., 2007. Changes of erosive rainfall for El Nino and La Nina years in the northern Andean highlands of Peru. Clim. Change 85, 343–356.
Ropelewski, C.F., Halpert, M.S., 1987. Global and regional scale precipitations patterns associated with El Nino-Southern Oscillation. Mon. Wea. Rev. 115, 1606–1626.
Ruiz, R.R., Torres, H.G., Aguirre, M.N., 2008. Delimitación y codificación de unidades hidrográficas del Perú. Autoridad Nacional del Agua-Ministerio de Agricultura, Lima- Perú (29 pp.).
Räisänen, J., Räty, O., 2013. Projections of daily mean temperature variability in the future: cross-validation tests with ENSEMBLES regional climate simulations. Clim. Dyn. 41, 1553–1568. http://dx.doi.org/10.1007/s00382-012-1515-9.
Räisänen, J., Ylhäisi, J., 2012. Can model weighting improve probabilistic projections of climate change? Clim. Dyn. 39, 1981–1998. http://dx.doi.org/10.1007/s00382-011-1217-8.
Räty, O., Räisänen, J., Ylhäisi, J., 2014. Evaluation of delta change and bias correction methods for future daily precipitation: intermodel cross-validation using ENSEMBLES simulations. Clim. Dyn. 42, 2287–2303. http://dx.doi.org/10.1007/s00382-014-2130-8.
Steele-Dunne, S., Lynch, P., McGrath, R., Semmler, T., Wang, S., Hanfin, J., Nolan, P., 2008. The impacts of climate change on hydrology in Ireland. J. Hydrol. 356, 28–45.
Swiech, T., Ertsen, M.W., Pererva, C.M., 2012. Estimating the impacts of a reservoir for improved water use in irrigation in the Yaramba region, Peru. J. Phys. Chem. Earth 47-48, 64–75.
Tapley, T.D.J., Waylen, P.R., 1990. Spatial variability of annual precipitation and ENSO events in western Peru. Hydrol. Sci. J. 35, 429–445.
Taylor, K.E., Stouffer, R.J., Meehl, G.A., 2012. An overview of cmip5 and the experiment design. Bull. Amer. Meteor. Soc. 93, 485–498. http://dx.doi.org/10.1175/bams-d-11-00094.1.
Thomson, D.J., 1982. Spectrum estimation and harmonic analysis. Proc IEEE 70, 1055–1096.
UNESCO, 2006. Balance hídrico superficial del Perú a nivel multianual. Documentos Técnicos del PHI-LAC, No1. Montevideo, 138 pp.
van Vuuren, D.P., Edmonds, J., Kainuma, M., Riahi, K., Thomson, A., Hibbard, K., Hurtt, G.C., Kram, T., Krey, V., Lamarque, J.-F., Masui, T., Meinshausen, M., Nakicenovic, N., Smith, S.J., Rose, S.K., 2011. The representative concentration pathways: an overview. Clim. Change 109 (1–2), 5–31. http://dx.doi.org/10.1007/s10584-011-0148-z.
Vauchel, P., 2005. HYDRACCESS: Software for Management and Processing of Hydro-meteorological Data. http://www.ore-hybam.org/index.php/Software/Hydraccess.
Veijalainen, N., Lotsari, E., Alho, P., Vehviläinen, B., Käyhkö, J., 2010. National scale assessment of climate change impacts on flooding in Finland. J. Hydrol. 391, 333–350.
Vergara, W., Deeb, A., Leino, I., Kitoh, A., Escobar, M., 2011. Assessment of the impacts of climate change on mountain hydrology: development of a methodology through a case study in the Andes of Peru. World Bank, Washington, DC (Accessed 10 May 2017).. http://documents.worldbank.org/curated/en/882751468295210584/Assessment-of-the-impacts-of-climate-change-on-mountain-hydrology-development-of-a-methodology-through-a-case-study-in-the-Andes-of-Peru.
Vuille, M., Bradley, R.S., Keimig, F., 2000. Interannual climate variability in the Central Andes and its relation to tropical Pacific and Atlantic forcing. J. Geophys. Res.-Atmos. 105, 12447–12460.
WBCSD, 2014. Water, food and energy nexus challenges. http://www.gwp.org/globalassets/global/toolbox/references/water-food-and-energy-nexus-challenges-wbcsd-2014.pdf. (Accessed 10 May 2017).
World Meteorological Organization (WMO), 2012. Standardized Precipitation Index User Guide. WMO, Geneva, Switzerland (ISBN 978-92-63-11091-6).
WWAP, 2015. The United Nations World Water Development Report 2015: Water for a Sustainable World. UNESCO, Paris.
Xu, C.-Y., 1999. Climate change and hydrologic models: a review of existing gaps and recent research developments. Water Resour. Manage. 13, 369–382.
Yates, D., Sieber, J., Purkey, D., Huber-Lee, A., Galbraith, H., 2005a. WEAP21: a demand, priority, and preference driven water planning model: part 2, Aiding freshwater ecosystem service evaluation. Water Int. 30 (4), 487–500.
Yates, D., Sieber, J., Purkey, D., Huber-Lee, A., 2005b. WEAP21: a demand, priority, and preference driven water planning model: part 1, model characteristics. Water Int. 30 (4), 501–512.